Journal of Inorganic Biochemistry 117 (2012) 261–269

Contents lists available at SciVerse ScienceDirect

Journal of Inorganic Biochemistry

journal homepage: www.elsevier.com/locate/jinorgbio

$[Ru^{II}(\eta^5\text{-}C_5H_5)(bipy)(PPh_3)]^+$, a promising large spectrum antitumor agent: Cytotoxic activity and interaction with human serum albumin

Ana Isabel Tomaz [a,*], Tamás Jakusch [b], Tânia S. Morais [a], Fernanda Marques [c], Rodrigo F.M. de Almeida [d], Filipa Mendes [c], Éva A. Enyedy [b], Isabel Santos [c], João Costa Pessoa [e], Tamás Kiss [b], M. Helena Garcia [a]

[a] Centro de Ciências Moleculares e Materiais, Departamento de Química e Bioquímica, Faculdade de Ciências da Universidade de Lisboa, Campo Grande 1749-016 Lisboa, Portugal
[b] Department of Inorganic and Analytical Chemistry, University of Szeged, P.O. Box 440, Szeged H-6701, Hungary
[c] Unidade de Ciências Químicas e Radiofarmacêuticas, Instituto Superior Técnico, Pólo de Loures - Campus Tecnológico e Nuclear, Universidade Técnica de Lisboa, Estrada Nacional 10, 2686-953 Sacavém, Portugal
[d] Centro de Química e Bioquímica, Departamento de Química e Bioquímica, Faculdade de Ciências da Universidade de Lisboa, Campo Grande 1749-016 Lisboa, Portugal
[e] Centro de Química Estrutural, Departamento de Engenharia Química, Instituto Superior Técnico, Universidade Técnica de Lisboa, Av. Rovisco Pais, 1049-001 Lisboa, Portugal

ARTICLE INFO

Article history:
Received 16 April 2012
Received in revised form 29 June 2012
Accepted 30 June 2012
Available online 6 July 2012

Keywords:
Ruthenium(II)
Cyclopentadienyl
Anti-tumor activity
Cytotoxicity
PARP-1 inhibitor
Human serum albumin-binding

ABSTRACT

Ruthenium complexes hold great potential as alternatives to cisplatin in cancer chemotherapy. We present results on the *in vitro* antitumor activity of an organometallic '$Ru^{II}Cp$' complex, $[Ru^{II}Cp(bipy)(PPh_3)][CF_3SO_3]$, designated as TM34 ($PPh_3$ = triphenylphosphine; bipy = 2,2′-bipyridine), against a panel of human tumor cell lines with different responses to cisplatin treatment, namely ovarian (A2780/A2780cisR, cisplatin sensitive and resistant, respectively), breast (MCF7) and prostate (PC3) adenocarcinomas. TM34 is very active against all tumorigenic cell lines, its efficacy largely surpassing that of cisplatin (CisPt). The high activity of TM34 towards CisPt resistant cell lines possibly suggests a mechanism of action distinct from that of CisPt. The effect of TM34 on the activity of the enzyme poly(ADP-ribose) polymerase 1 (PARP-1) involved in DNA repair mechanisms and apoptotic pathways was also evaluated, and it was found to be a strong PARP-1 ruthenium inhibitor in the low micromolar range ($IC_{50} = 1.0 \pm 0.3$ μM). TM34 quickly binds to human serum albumin forming a 1:1 complex with a conditional stability constant (log K′~4.0), comparable to that of the Ru^{III} complex in clinical trial KP1019. This indicates that TM34 can be efficiently transported by this protein, possibly being involved in its distribution and delivery if the complex is introduced in the blood stream. Albumin binding does not affect TM34 activity, yielding an adduct that maintains cytotoxic properties (against A2780 and A2780cisR cells). Altogether, the properties herein evaluated suggest that TM34 could be an anticancer agent of highly relevant therapeutic value.

© 2012 Elsevier Inc. All rights reserved.

1. Introduction

Cancer is the second largest cause of death in developed countries, and the number of worldwide deaths from cancer is projected to rise to over 13.1 million people in 2030 according to the World Health Organization predictions [1]. Statistically, two in five men and women born today (41.21%) will be diagnosed with cancer at some stage during their lifetime [2].

The discovery of the anticancer properties of cisplatin by Rosenberg and co-workers [3] paved the way for the development of metal-based cancer chemotherapy. To date, cisplatin, carboplatin and oxaliplatin are the only worldwide approved metal-based chemotherapeutic agents in clinical use [4,5] despite their high toxicity and incidence of resistance to treatment, which severely limit their clinical value. Ruthenium complexes are now a proven effective alternative to Pt-based complexes in cancer chemotherapy, affording different mechanisms of action, a different spectrum of activity and the potential to overcome platinum-resistance, as well as lower toxicity [6–11]. Despite the fact that full development of a ruthenium complex into a commercially available drug has not been reached, two leading examples completed phase I in clinical trials, namely KP1019 ([HInd][*trans*-$Ru^{III}Cl_4(Ind)_2$], Ind = indazole) [12] and NAMI-A ([HIm][*trans*-$Ru^{III}Cl_4$(DMSO)Im], Im = imidazole) [13] with several other different families currently undergoing scrutiny for their chemotherapeutic potential [11,14–16].

Organometallic mononuclear piano-stool '$Ru(\eta^6\text{-}C_6H_6)$' structured complexes are probably the most numerous group of Ru(II)-compounds reported as potential metallodrugs [15]. A review of the extensive work on ruthenium η^6-arene derivatives was recently published highlighting the scope of these agents as metallodrugs [17–19]. One of the most striking features of Ru-compounds is the anti-metastatic effect that some of the complexes of this class present, with the octahedral Ru^{III} NAMI-A and the piano-stool Ru^{II} RAPTA-T ($[Ru^{II}Cl_2(\eta^6\text{-toluene})(PTA)]$, PTA = 1,3,5-triaza-7-phosphaadamantane) being the most studied [11,15,16].

Fewer studies are reported in the literature for the related isoelectronic Ru(II)-cyclopentadienyl derivatives. '$Ru(\eta^5\text{-}C_5H_5)$' compounds, where the half-sandwich metal moiety works as a scaffold, were

* Corresponding author. Tel.: +351 217 500 949; fax: +351 217 500 088.
E-mail address: isabel.tomaz@fc.ul.pt (A.I. Tomaz).

0162-0134/$ – see front matter © 2012 Elsevier Inc. All rights reserved.
doi:10.1016/j.jinorgbio.2012.06.016

successfully explored for the development of potent and selective kinase inhibitors [20–22]. The water soluble organometallic complex $[Ru^{II}Cp^{*}Cl(PTA)_2]$ (Cp^{*} = pentamethylcyclopentadienyl) showed good activity as an inhibitor of specific tumor cell proliferation on TS/A murine adenocarcinoma cells [23], and a series of ionic Ru^{II}(arene)Cp^{*} sandwich complexes exhibited a promising anticancer activity with IC_{50} values comparable to (but not surpassing) that of cisplatin [24].

We developed a mixed sandwich structured family of {$Ru^{II}Cp(\eta^6$-arene)} compounds, where the η^6-arene planar system was chosen to target DNA by promoting an intercalative mechanism of interaction, which surprisingly revealed only moderate cytotoxicity against leukemia cells, in spite of the strong plasmid DNA interaction observed by atomic force microscopy (AFM) [25].

In our approach to ruthenium metallodrugs for cancer chemotherapy we also reported a new family of ruthenium(II) organometallic prospective drugs of general formula $[Ru^{II}Cp(PP)L]^{+}$, L being a nitrogen σ-bonded N-heterocyclic ligand (1,3,5-triazine, pyridazine) and PP a phosphane ligand (1,2-bis(diphenylphosphane)ethane, triphenylphosphane) which exhibited excellent cell viability inhibition of LoVo human colon adenocarcinoma and MiaPaCa pancreatic cell lines [26], with IC_{50} values in the sub-micromolar range. A second set of 'Ru^{II}(Cp)' half-sandwich complexes with an N-heterocyclic σ-bonded ligand (imidazole; 5-phenyl-1H-tetrazole), or N-cyano ligand (benzo[1, 2-b; 4,3-b]dithio-phen-2-carbonitrile; [5-(2-thiophen-2-yl)-vinyl]-thiophene-2-carbonitrile) also exhibited excellent activity in the sub-micromolar range against HL-60 cells [27], within the lowest values reported for piano stool Ru-complexes. In addition, all complexes of this set induced cell death mainly by apoptosis. Varying the denticity of L or of PP co-ligand in the '$Ru^{II}Cp$' center yielded equally efficient agents active in the sub-micromolar range against leukemia cells, apoptosis being the major mechanism of cell death for all compounds tested [27,28].

In our extensive family of '$Ru^{II}Cp$' compounds we found particularly interesting features for the complex $[Ru^{II}(\eta^5\text{-}C_5H_5)(bipy)(PPh_3)]^{+}$ (PPh_3 = triphenylphosphane; bipy = 2,2′-bipyridine), isolated as the $CF_3SO_3^{-}$ salt, that for simplicity we will refer to as TM34 (Scheme 1) [28]. This complex with IC_{50} values of (3.30 ± 0.83) μM and (0.42 ± 0.25) μM for a 24 h and 72 h incubation period, respectively, was *ca.* five times more active towards HL-60 cells than cisplatin. Furthermore, TM34 induced the same percentage of apoptotic (35.9%) and damaged or necrotic cells (1.1%) as cisplatin (37.2% and 1.4%, respectively) [28]. AFM images on pBR322 DNA incubated with TM34 displayed several supercoiled forms of plasmid DNA, and were similar to images previously observed for typical intercalating molecules [29], showing that this agent was able to strongly modify the DNA structure [28]. Nevertheless, the extent of DNA interaction if considered alone does not correlate well with the high cytotoxic activity observed within the {$Ru^{II}(\eta^5\text{-}C_5H_5)$} family of compounds, which suggested that other biological targets might be involved in the mechanism of action.

In the present work we explore the potential of TM34 as an anti-cancer metallodrug by screening its activity against a panel of several human tumor cell lines. The increasing evidence in the literature of the importance of enzymes and proteins as relevant targets for the mode of action of non-platinum anticancer metallodrugs (for which multiple biological pathways have been proposed) [30–33] led us to explore the role of proteins in the anti-tumor activity of TM34. PARP inhibitors have been considered as drugs for use in combinatorial therapies with alkylating agents [34] and to sensitize cancer cells to subsequent treatment with cisplatin and carboplatin [35–38].

A recent report on the inhibition activity of PARP-1 by cisplatin, NAMI-A and RAPTA-T showed that all these metallodrugs inhibited the activity of the enzyme more efficiently than the benchmark inhibitor 3-aminobenzamide, highlighting the role this interaction plays in their mode of action [39]. In this context and to further understand the mechanism of cell death promoted by this compound, the effect of TM34 in PARP-1 inhibition was also assessed.

The bioavailability of any prospective drug is of crucial importance when screening potential pharmaceuticals. Drug binding to plasma proteins can exert a significant effect on its distribution and pharmacokinetics [40,41], and an evaluation of the binding to serum proteins is now a requirement of the FDA as part of the drug development process [42]. The relevance of human serum albumin (HSA) interaction in drug delivery should also be highlighted in a different scope. Albumin is known to accumulate in malignant and inflamed tissue due to a leaky capillary system combined with an absent or defective clearance system, and this enhanced permeability and retention effect (EPR effect) can be used to access more efficient tumor-selective drug delivery [43,44]. In this context, and as an initial approach to outline the pharmacokinetics of TM34, we investigated its interaction with human serum albumin as a vehicle for the transport in the blood plasma and eventual passive targeting, and assessed the activity of a {protein-complex} adduct eventually formed.

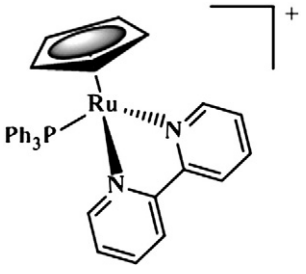

Scheme 1. Chemical structure of $[Ru^{II}(\eta^5\text{-}C_5H_5)(bipy)(PPh_3)]^{+}$ (TM34).

2. Experimental section — materials and methods

2.1. General

All chemical reagents were used as received from the supplier without further purification. Fatted HSA (from human plasma, A1653; 96–99%) with a molecular mass of 66–67 kDa was purchased from Sigma-Aldrich. The complex TM34 was synthesized as reported previously [28]. Millipore® water was used for the preparation of the solutions, and 10 mM 4-(2-hydroxyethyl)-1-piperazineethanesulfonic acid (Hepes) buffer (Sigma-Aldrich) with 0.15 M NaCl (Sigma-Aldrich) was used in all experiments involving spectroscopic measurements. This buffer system was adjusted to pH 7.4 using KOH and/or HCl solutions.

2.2. Sample preparation of complex—HSA complexes

Stock solutions of human serum albumin were prepared by gently dissolving the protein in pH = 7.4 Hepes buffer (10 mM). 30–60 min was needed to allow the protein to hydrate and fully dissolve, being gently swirled from time to time. The concentration of each HSA stock solution was determined by UV spectrophotometry using the molar extinction coefficient ε(278 nm) = 36,850 M^{-1} cm^{-1} [45–48]. Individual protein-complex samples were prepared to ensure in each assay the same incubation time at (37 ± 1) °C. Due to the limited solubility of the complexes in aqueous media, dimethylsulfoxide (DMSO, from Sigma-Aldrich) was used to prepare concentrated stock solutions of each complex, following appropriate dilution (also in DMSO) to obtain the desired complex concentration and the same % DMSO in the final samples. All stock solutions were prepared and dilutions were carried out immediately prior to sample preparation. The DMSO content was kept to a maximum of 2% (v/v) in pH 7.4 10 mM Hepes buffer/0.15 M NaCl in all samples.

2.3. Ultrafiltration–UV–visible (UV–vis) measurements

For ultrafiltration measurements 500 μL samples in 2% DMSO/10 mM Hepes pH 7.4 buffer were prepared in different experimental conditions. The complex concentrations used were 10, 20 and 50 μM, and were kept constant within each series while varying the complex-to-protein molar ratios. These were 1:1 (for 10 and 20 μM TM34 concentrations), and ranged from 1:1 to 1:3 in 50 μM essays. Incubation time was 40 min or 30 min at 25 °C and 37 °C, respectively. Controls with the same analytical concentration of complex (2 or 3 *per* complex concentration used) but with no protein were prepared and incubated in the same conditions as the samples. The HSA and HSA-bound complexes were then separated from the low molecular mass fraction (LMM) containing the non-bound complex TM34 with a temperature-controlled centrifuge (Sanyo, 10,000/s) through 10 kDa membrane filters (Microcon YM-10, Millipore®).

Samples and controls were centrifuged for 15 min at the same temperature as in the incubation conditions. Care was taken to avoid extending the centrifugation time for too long as to allow drying of the high molecular fraction in the membrane filter. LMM fractions (from 2 filters with the same sample composition) were combined and diluted 1:2 to a final volume of 1.0 mL, and the concentration of the free Ru-complex was determined by UV–vis spectrophotometry. Spectra of the LMM fractions were always compared to that of the corresponding controls (with the same analytical complex concentration).

2.4. Spectroscopic measurements

UV–vis absorption spectra were recorded at room temperature on a Hitachi U2000 or a Hewlett Packard 8452A diode array spectrophotometer in the range 270/300–800/900 nm with 1 cm path quartz Suprasil® cuvettes.

Fluorescence measurements were carried out on a Spex Fluorolog® 3-22/Tau-3 spectrofluorometer from Horiba Jobin Yvon at room temperature (23 ± 2 °C). For these measurements, the final protein concentration in the (individually prepared) samples was 1.0 μM (constant), and the complex concentration was varied accordingly to obtain HSA-to-Ru-complex molar ratios ranging from 1:0.5 to 1:25. Incubation times at 37 °C were 3 h and 24 h. Samples with the same complex concentration but with no protein were prepared for appropriate background correction.

For steady-state fluorescence intensity measurements excitation was done at 295 nm. Fluorescence emission intensity was corrected for the absorption and emission inner filter effects [49,50] using (UV–vis) absorption data recorded for each sample. Bandwidth was typically 5 nm in both excitation and emission. For time-resolved measurements by the single photon counting technique a nanoLED N-280 (Horiba Jobin Yvon) was used for the excitation of HSA, and the emission wavelength was 340 nm with a 10 nm bandwidth. Ludox® (from Sigma-Aldrich) was used as the scatterer to obtain the instrumental response function. The program TRFA data processor version 1.4 (Minsk, Belarus) was used for the analysis of the experimental fluorescence decays. The fluorescence intensity decays were analyzed by fitting a sum of exponentials according to

$$I(t) = \sum_{i=1i}^{n} \alpha_i \exp(-t/\tau_i) \quad (1)$$

where α_i and τ_i are the normalized amplitude and lifetime of component i, respectively. The mean fluorescence lifetime was obtained through Eq. (2),

$$\langle \tau \rangle = \sum_{i=1}^{n} \alpha_i \tau_i^2 / \sum_{i=1}^{n} \alpha_i \tau_i. \quad (2)$$

The changes in quantum yield by processes affecting fluorescence lifetime were evaluated from the amplitude-weighted mean fluorescence lifetime, which is given by

$$\bar{\tau} = \sum_{i=1}^{n} \alpha_i \tau_i. \quad (3)$$

The quality of fit was evaluated by a reduced χ^2 value close to 1 and random distribution of weighted residuals and residual autocorrelation.

2.5. Calculations

Experimental data obtained from the TM34–HSA interaction was used to calculate conditional stability binding constants for {protein ↔ Ru-complex} adducts formed according to:

$$\mathrm{HSA} + n(\mathrm{Ru-complex}) \rightleftarrows \{(\mathrm{HSA})\text{–}(\mathrm{Ru-complex})n\}$$

using the PSEQUAD computer program [51] by a procedure described in detail in a previous publication on ultrafiltration and fluorescence binding data by Enyedy and co-workers [52]. The uncertainty in the calculated stability constants is taken as 3 times the standard deviation (SD) obtained in the calculations.

(UV–vis) electronic spectra in the range 296–492 nm of the LMM fractions separated by ultrafiltration were used as a measure of the free (unbound) Ru-complex obtained at different protein-to-complex ratios. The formation of only one adduct with 1:1 stoichiometry ($n = 1$) initially proposed was found to describe the experimental UV-vis and fluorimetric data quite well, and the corresponding conditional binding constant ($\log K'_B$) was calculated with the computer program PSEQUAD.

In the case of the fluorescence data, emission spectra in the range 305–450 nm were corrected for both the excitation and emission inner filter effects prior to the calculations.

2.6. Cell studies

2.6.1. Cell culture

Cell lines (obtained from ATCC) used in this study were four human cancer cell lines with different responses to cisplatin (CisPt) treatment: A2780 and A2780cisR human ovarian adenocarcinoma (CisPt sensitive and resistant, respectively), PC3 human grade IV prostate carcinoma, MCF7 human breast adenocarcinoma, and one non-tumorigenic cell line (V79 Chinese hamster lung fibroblasts). The cells were maintained in DMEM (Dulbecco's modified Eagle's medium, Invitrogen) containing GlutaMax 1 (MCF7) or RPMI 1640 (A2780/A2780cisR, PC3 and V79) supplemented with 10% FBS and 1% penicillin/streptomycin (Invitrogen). All cell lines were kept in a CO_2 incubator (Heraus, Germany) with 5% CO_2 at 37 °C in a humidified atmosphere. Cells from a confluent monolayer were removed from flasks by a trypsin–EDTA solution and seeded in multi-well culture plates. For experimental purposes the cellular viability was first checked by the trypan blue dye exclusion test, and then cells were suspended in medium and seeded in multi-well plates.

2.6.2. Cytotoxicity assays

The cytotoxic activity of TM34 was screened against all cell lines within the concentration range 10^{-10}–10^{-4} M using the MTT [3-(4,5-dimethylthiazol-2-yl)-2,5-diphenyltetrazolium bromide] colorimetric assay [53]. For the cytotoxic evaluation cells were seeded in 200 μL of complete medium in 96-well plates. The plates were incubated at 37 °C for 24 h prior to complex testing to allow cell adhesion. The stock solution in DMSO (20 mM) of the complex was freshly prepared and used for sequential dilutions in complete medium. The final concentration of DMSO in the cell culture medium did not exceed 0.5%. Control groups with and without DMSO (0.5%) were included in the assays. The commercial metallodrug cisplatin was included in this study as a positive control.

Analysis of cell survival was carried out after a 72 h cell exposure to the complex by the MTT colorimetric assay which is based on the reduction of MTT by viable cells to form formazan crystals. Briefly, a solution of MTT dissolved in PBS (0.5 mg/mL) was added to each well (200 μL) and the plates were incubated at 37 °C for 3–4 h. Then the medium was discarded and 200 μL of DMSO was added to each well to dissolve the formazan crystals. The absorbance was measured at 570 nm with a plate spectrophotometer (Power Wave Xs, Bio-TeK). Each experiment was repeated at least three times and each concentration was tested in at least six replicates. Results are expressed as a percentage of survival with respect to control cells in the absence of the compound. IC_{50} values (half-inhibitory concentration, *i.e.* drug concentration that induces 50% of cell death) were calculated from curves constructed by plotting cell survival (%) *versus* compound concentration (M). The IC_{50} values were calculated with the GraphPad Prism software.

2.6.3. Effect of HSA on the cytotoxicity of TM34

The effect of albumin (HSA) on cell viability of A2780 and A2780cisR cells, either alone or in combination with the TM34 complex, was evaluated using 1 μM (and 5 μM in the first case) of TM34. The complex was pre-incubated with different HSA concentrations for 20 min at 37 °C prior to the cell treatment, at compound-to-protein molar ratios of 1:1, 1:5 and 1:10. A2780/A2780cisR cells were seeded on 96-well plates 24 h before incubation with TM34 samples in complete medium containing 5% of FBS [55]. After a 24 h incubation period the treatment solution was removed, and the cell viability was measured by the MTT assay.

2.7. PARP-1 activity assay

PARP-1 activity was determined using Trevigen's HT Universal Colorimetric PARP assay. This assay measures the incorporation of biotinylated poly(ADP-ribose) onto histone proteins in a 96 microtiter strip well format. Recombinant human PARP-1 (high specific activity) was used as the enzyme source. 3-Aminobenzamide (3-AB) was used as a control inhibitor. The final reaction mixture (50 μL) was treated with TACS-Sapphire™, a horseradish peroxidase colorimetric substrate, and incubated in the dark for 30 min. Absorbance was read at 630 nm after 30 min. The data are means of at least three experiments done in triplicate ± SD (SD is the standard deviation).

3. Results and discussion

3.1. Complex solubility and stability in aqueous media

The complex is highly soluble in methanol and non-protic solvents such as dichloromethane, acetone and DMSO, but exhibited low solubility in both water and buffered aqueous media.

The stability of TM34 in aqueous media was tested by UV–vis (in DMSO and 2% DMSO/pH 7.4 Hepes buffer) and by ^{1}H and ^{31}P NMR (in DMSO-d_6) spectroscopy.

The (UV–vis) absorption spectrum of TM34 in dichloromethane was previously reported to have two intense absorption bands attributed to the $[Ru(Cp)(PPh_3)]^+$ moiety and coordinated bipy chromophore in the UV range (240–340 nm), with two additional bands (423 nm and 475 nm) assigned to metal-to-ligand charge transfer transitions from the Ru-4d orbitals to π* in the bipyridine ring [28].

The spectrum in DMSO shows distinctly the intense absorption band (λ_{max} = 288 nm, ε = 40,021 M^{-1} cm^{-1}) and a lower intensity band (λ = 416 nm, ε = 4435 M^{-1} cm^{-1}), with two additional shoulders at ~345 nm (ε ~ 6000 M^{-1} cm^{-1}) and ~462 nm (ε ~ 2550 M^{-1} cm^{-1}).

Changes observed in the UV–vis spectrum of TM34 over a 30 h period were negligible, indicating that the complex is quite stable in a strong coordinating solvent such as DMSO (Fig. S-1). This was further supported by NMR spectroscopy. Both in the ^{1}H NMR (in DMSO-d_6; δ (chemical shift)/ppm, m = multiplet, d = doublet, s = singlet: 4.87 [s, 5H, η^5-C_5H_5], 6.93–6.97 [m, 6H, $H_{orto}(PPh_3)$], 7.26–7.32 [m, 7H, bpy + $H_{meta}(PPh_3)$], 7.38–7.40 [m, 3H, $H_{para}(PPh_3)$], 7.85 [t, 2H, bpy], 8.18 [d, 2H,bpy], 9.37 [d, 2H, bpy]) and in the ^{31}P NMR (DMSO-d_6; δ/ppm: 51.7 [s, PPh_3]) spectra of the complex, no changes in δ values were detected from the mixing time up to 24 h (data not shown). The data confirms the stability of TM34 in strong coordinating solvents indicating that it is possible to prepare stock solutions in DMSO with no complex decomposition.

Solubility in water at a ~200–500 μM concentration could be achieved using a small % of DMSO in buffered aqueous medium. In 2% DMSO/98% pH 7.4 10 mM Hepes buffer the UV–vis spectrum of TM34 exhibits similar features as in pure DMSO solvent: λ_{max} = 289 nm (ε = 17,766 M^{-1} cm^{-1}), a shoulder at ~345 nm (ε ~ 4270–4275 M^{-1} cm^{-1}), λ = 410 nm (ε = 3346 M^{-1} cm^{-1}) and a second shoulder at ~455 nm (ε ~ 1700 M^{-1} cm^{-1}). The stability of the complex was evaluated over time by UV–vis spectroscopy at room temperature, in the presence and absence of light. Only negligible changes could be observed in its spectrum up to ~30 h (Fig. 1), with a maximum of a 5% variation in the spectrum intensity after *ca.* 24 h, indicating that the complex stability in aqueous solution is quite adequate for *in vitro* biological evaluation as well as quantitative determination of binding constants.

3.2. In vitro cytotoxicity

The cytotoxic activity of TM34 was evaluated as the IC_{50} value in four human tumor cell lines (A2780, A2780cisR, MCF7 and PC3) and in the non-tumorigenic V79 cell line, within the concentration range 10^{-10}–10^{-4} M. The panel of cell lines chosen comprises human tumor cells with different sensitivities to the treatment with cisplatin, and includes the most frequent cancer conditions diagnosed in women (breast cancer) and men (prostate cancer). The metallodrug in clinical use cisplatin was used as a positive control, and the MTT assay was also carried out for the reference drug in the same concentration range after a 72 h cell exposure for comparative purposes. Results are summarized in Table 1, and Figs. S-2 and S-3.

TM34 exhibits high cytotoxicity against all tumor cell lines studied exhibiting IC_{50} values in the sub-micromolar range, largely surpassing the activity of cisplatin especially against the resistant cell lines. In particular, TM34 was found to be 17 times more active against A2780, while also being ~200-folds more cytotoxic against A2780cisR, and 100-folds more active in the case of the resistant cell lines MCF7 and PC3 when compared with CisPt. Moreover, the IC_{50} value found for the non-tumorigenic V79 cell line was 7- to 60-times higher (for PC3 and A2780cisR, respectively) which suggests some intrinsic selectivity of TM34 towards cancer cells (Table 1, Fig. S-2).

The finding that TM34 is active in the sub-micromolar range and especially towards CisPt resistant cell lines suggests a mechanism of action different from that of CisPt, and makes this complex particularly interesting for further study.

3.3. PARP-1 inhibition

PARP enzymes (poly-(adenosine diphosphate (ADP)-ribose) polymerases) play a key role in DNA repair mechanisms by detecting and initiating repair after DNA strand breaks [56]. PARP inhibitors have been evaluated as drugs for use in combinatorial therapies with DNA-damaging agents [34] and to sensitize cancer cells to subsequent treatment with cisplatin and carboplatin [35–38]. Phase I and II clinical trials evaluating the use of PARP inhibitors in combination therapies with platinum drugs are currently underway [57]. PARP-1, the most studied member of the PARP family, is activated by mild DNA damage and is involved in the DNA repair process, so that the cell survives. However, in the case of extensive DNA damage, PARP-1 is overactivated and induces a depletion of cellular NAD^+ and ATP

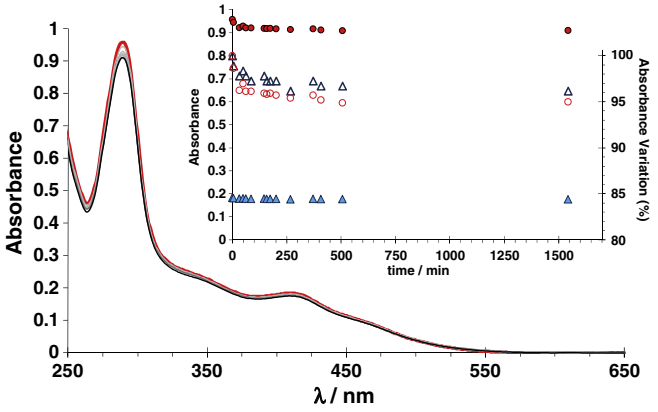

Fig. 1. Evaluation of complex stability in 2% DMSO/10 mM Hepes pH 7.4. UV–visible spectra recorded over time, from 2 min (orange) up to 1540 min = 25.7 h (black), for a 53.2 μM DMSO solution of TM34; *inset*: absorbance at the two maximum absorption intensity bands over time (*left axis*, 289 nm, red closed circle; 410 nm, blue closed triangle) and % change observed in absorbance values (*right axis*, 289 nm, open red circle; 410 nm, open blue triangle) over the same period.

levels leading to cell dysfunction or eventually to necrotic cell death [58–61]. Moreover, PARP-1 may cause cellular death *via* necrosis or apoptosis, depending on the type, strength and duration of genotoxic stimuli as well as the cell type. The cytotoxic activities of ruthenium and gold compounds have recently been related to a very strong inhibition in the sub-nanomolar range on the purified PARP-1 enzyme and on protein extracts from tumor cell lines [39,62].

PARP-1 expression is upregulated in various types of human cancers [63]. In cancer cells with selective defects in homologous recombination repair, inactivation of PARP directly causes cell death, and this phenomenon can be employed to specifically target tumor cells while sparing healthy tissues [63]. Apoptosis had previously been found to be the major mechanism of cell death exerted by TM34 and, in this context, it is quite relevant to evaluate this complex as a possible PARP inhibitor.

PARP-1 inhibition was determined on the purified human enzyme. Inhibition activity is evaluated in terms of the half-inhibitory concentration value, IC_{50}. The enzyme was incubated with TM34 at varying concentrations, for 2 h and 24 h, before assessing its activity spectrophotometrically by measuring the incorporation of biotinylated poly(ADP-ribose) onto histone proteins (see Experimental section).

The resulting IC_{50} values at 24 h are reported in Table 2 in comparison to the PARP-1 reference inhibitor 3-AB (3-aminobenzamide) [64]. No difference in the results was observed between the long and short incubation periods (2 h *versus* 24 h) — Fig. 2.

The ruthenium complex TM34 presents an IC_{50} value for PARP inhibition of 1 μM, substantially lower than that of the classical inhibitor 3-AB. The Ru-complexes RAPTA-T and NAMI-A also exhibit low IC_{50} values (28 and 18.9 μM, respectively), somewhat higher than cisplatin (12.3 μM) [39]. Comparing these metallodrugs, TM34 is the strongest ruthenium inhibitor of PARP-1, its effect clearly surpassing those of RAPTA-T and NAMI-A, and that of cisplatin as well (these being *ca.* 30- to 10-times less effective).

3.4. Interaction with HSA

HSA is the most important non-specific transport vehicle in the blood plasma with an extraordinary ability to bind both endogenous metabolic compounds and exogenous therapeutic drugs, providing a depot for a wide variety of compounds (which may thus be available at concentrations higher than their solubility in the plasma) or a clearance route (which may prevent the compound to exert its therapeutic effect). It can increase, slow down or prevent passive extravasation into tissues and thus exert a significant effect on the drug actual performance *in vivo* [40,41,43]. In addition, HSA can provide passive targeting to tumor tissues as a consequence of the EPR effect [43,44].

The binding of TM34 to human serum albumin is a first approach to outline its pharmacokinetics, and was investigated by spectroscopic methods (absorption and fluorescence) and ultrafiltration–UV–vis.

The UV–vis spectrum of TM34 in the absence and in the presence of HSA did not exhibit characteristic features that would clearly indicate an interaction between the compound and the protein. For a 1:2 complex-to-protein molar ratio (for $C_{TM34} = 19.6$ μM, 60 min incubation) a modest 7.5% hyperchromism (410 nm) was observed in the spectrum of the complex compared to the sum of the spectra recorded for the complex alone and the protein alone, with no other detectable changes.

3.4.1. Ultrafiltration–UV–vis measurements with spectrophotometric detection

The direct interaction of TM34 and HSA was studied by means of ultrafiltration/UV–vis experiments, using samples with the same complex concentration and different metal complex-to-protein molar ratios in each assay, and different TM34 total concentrations (C_{TM34}). The non-bound fraction (low molecular mass fraction, LMM) was separated from HSA and HSA-bound complexes (collected in the high molecular fraction).

Different incubation times were initially tested (from 15 min to 1 h) and this parameter optimized for an ~30 min contact time (for $C_{TM34} =$ 50 μM, 1:1 molar ratio, 37 °C), since higher incubation times resulted in negligible increase of the unbound concentration of the complex (not shown). The UV–vis spectra of the LMM fractions were compared to the reference spectra of TM34 alone with samples treated in the same way (Fig. 3), the ratios of the non-bound and of the total amount of complex were obtained, and data were analyzed with the help of the PSEQUAD computer program. The conditional stability constants obtained for the formation of a 1:1 {TM34–HSA} adduct from ultrafiltration–UV–vis results at 25 °C and at 37 °C are reported in Table 3. At pH 7.4 binding

Table 1
In vitro cytotoxic activity measured as the half-inhibitory concentration (IC_{50}) for the complex TM34 against several human tumor cell lines after a 72 h incubation period: A2780 and A2780cisR (cisplatin sensitive and resistant, respectively, ovarian adenocarcinoma), MCF7 (breast adenocarcinoma) and PC3 (prostate adenocarcinoma). V79 is a non-tumorigenic cell line (Chinese hamster lung fibroblasts). IC_{50} values are reported in μM (± SD), and incubation times are indicated. The reference metallodrug in clinical use cisplatin was used as a positive control.

	IC_{50}/(μM)				
Cell line	A2780	A2780cisR	MCF7	PC3	V79
TM34	0.14 ± 0.01	0.07 ± 0.02	0.29 ± 0.01	0.54 ± 0.10	4.21 ± 1.50
Cisplatin	2.5 ± 0.3	14 ± 2.2	28 ± 6[a]	51 ± 7[a]	–

[a] Taken from [54] obtained with the same experimental conditions and included here for comparison.

Table 2
IC_{50} values for PARP-1 inhibition following a 24 h incubation.

Compound	IC_{50}/μM[a]
TM34	1.0 ± 0.3
RAPTA-T	28 ± 2[b]
NAMI-A	18.9 ± 1.6[b]
Cisplatin	12.3 ± 2.0
3-AB	33[c]

[a] Values are the mean ± SD of at least three determinations done in triplicate.
[b] From [39].
[c] From [64].

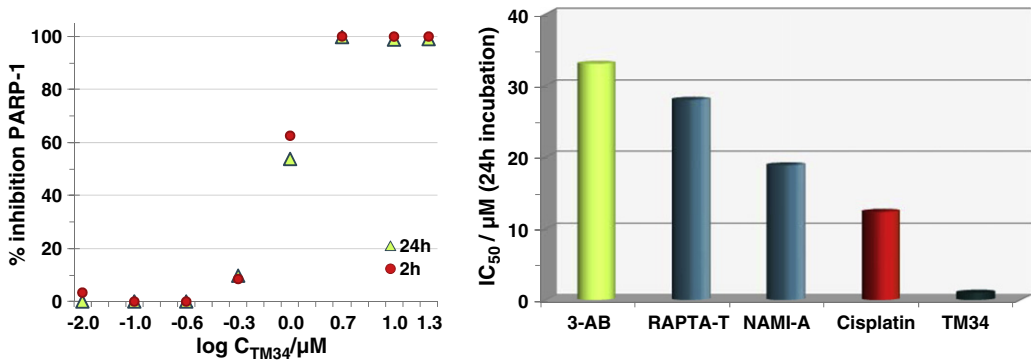

Fig. 2. PARP-1 inhibition by complex TM34. *Left*: time-dependence of PARP-1 activity on the concentration of complex TM34; incubation time at 37 °C is indicated, 2 h (red circles) and 24 h (green triangles). *Right*: IC_{50} value for TM34 inhibition compared to the reference benchmark PARP-1 inhibitor 3-AB (3-aminobenzamide) [62], to cisplatin, and to ruthenium complexes that exhibit antimetastatic activity *in vivo* NAMI-A and RAPTA-T (data for comparison taken from [39]) (see Table 2).

of TM34 to HSA is a fast process with a binding constant of $10^{4.2}$ after a 40–30 min incubation. Surprisingly, there is no measurable difference in log K values calculated for 25 °C and 37 °C, indicating that the binding process is rather independent of the incubation temperature in the temperature range studied, possibly due to the relatively strong heat resistance of this serum protein preserving the binding properties.

3.4.2. Steady-state and time-resolved fluorescence measurements

HSA exhibits intrinsic fluorescence due to the presence of its phenylalanine, tyrosine and tryptophan (Trp) residues, of which Trp is the dominant intrinsic fluorophore [65], and can be selectively excited at $\lambda_{exc} = 295$ nm. HSA contains a single Trp residue, Trp214, and its position in the protein is well defined: Trp214 is located in subdomain IIA, near Sudlow's drug binding site I [66,67]. Trp214 is very sensitive to its local environment, and its emission fluorescence easily responds to small changes in the vicinity of the indole ring that occur in response to *e.g.* substrate binding or denaturation (among other processes) [65]. This feature is quite valuable to probe HSA ↔ metallodrug interactions using fluorescence spectroscopy.

In this study, fatty-acid-containing HSA (extracted from human plasma) was used to evaluate the potential of the protein to bind the Ru^{II}-complex *in vivo*, since binding of fatty acids is known to modify the ability of this protein to bind other compounds due to conformational changes that render some binding sites unavailable [40,41,68].

A DMSO content as low as 2% affects the fluorescence emission of Trp214, decreasing it to *ca.* 10% as compared with the emission of the protein in the same medium with no DMSO, and no spectral shifts being observed. In this study, HSA alone solutions (prepared from stock solutions with no DMSO) always contained the same amount of DMSO as the samples and blanks, and care was taken to add DMSO to both samples and HSA at the same time.

In the absence of complex the emission maximum intensity for Trp214 is observed at 334 nm, showing that in the protein this residue is protected from the aqueous solvent, where Trp would have a maximum emission at *ca.* 350 nm [65]. Fig. 4 shows the effect of increasing concentration of TM34 on the protein fluorescence: quenching of the fluorescence emission intensity is observed, with no shift in the maximum λ_{em}.

The high overlap between the TM34 absorption spectrum and the HSA-Trp214 emission spectrum makes it possible for reabsorption of emitted light [69]. In addition TM34 exhibits a strong absorption band at $\lambda_{exc} = 295$ nm, with considerable absorbance values at 340 nm (λ_{em}^{max}) and hence data must be corrected for inner filter effects (IFE) at both excitation and emission wavelengths to account for these features that decrease the steady-state fluorescence intensity and are not due to a real interaction [50,70,71].

Stern–Volmer plots provide information on the mechanism causing the quenching observed, and are presented in Fig. 4.B (for $\lambda_{em}^{max} =$ 340 nm). Corrected I_{F0}/I_F data resulting from steady-state measurements are shown in open circles (○). The variation of I_{F0}/I_F with increasing complex concentration follows a linear trend and fits reasonably ($R^2 = 0.9941$) to the equation

$$\frac{I_{F0}}{I_F} = (1.001 \pm 0.003) + (10.5 \pm 0.4) \times 10^3 \times (c_{TM34}/M).$$

The Stern–Volmer plot for time-resolved fluorescence measurements, $\bar{\tau}_0/\bar{\tau}$ *versus* C_{TM34} is included in Fig. 4.B, showing that the amplitude-weighted mean fluorescence lifetime $\bar{\tau}$ remains unchanged in the presence and absence of the complex (see Fig. 5), which implicates

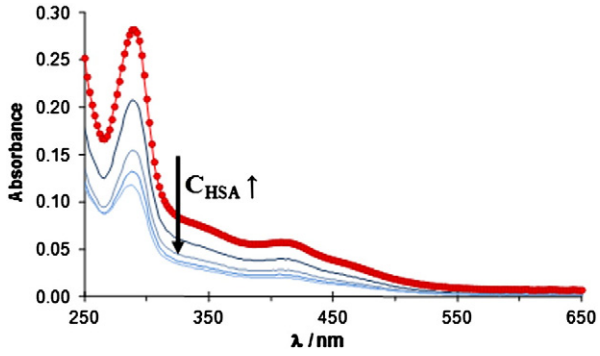

Fig. 3. UV–vis spectra of the LMM fraction collected for unbound TM34 complex at different HSA-to-Ru(II) complex molar ratios in 2% DMSO/10 mM Hepes pH 7.4/0.15 M NaCl. Reference spectrum recorded from controls with no protein for $C_{TM34} = 50$ μM (red line with red circles), spectra obtained from samples with C_{HSA} of 50, 75, 100 and 150 μM at the same complex concentration (blue line); samples were incubated in the dark for 30 min at 37 °C; the arrow indicates changes in absorbance with increasing protein ratio.

Table 3
Conditional stability constants (K_B') obtained for the HSA–TM34 system in 2% DMSO/10 mM Hepes pH 7.4/0.15 M NaCl. SD = standard deviation.

Method	Incubation conditions		Spectral range[a] Δλ/nm	Log $K_B' \pm 3SD$
	T/°C	Time		
Ultrafiltration–UV	25	40 min	296–492	4.15 ± 0.02
	37	30 min	(PSEQUAD)	4.16 ± 0.03
Steady-state fluorescence	37	3 h	340 (Stern–Volmer plot)	4.02 ± 0.02
			306–450 (PSEQUAD)	3.94 ± 0.01

[a] Spectral range considered for K_B calculations.

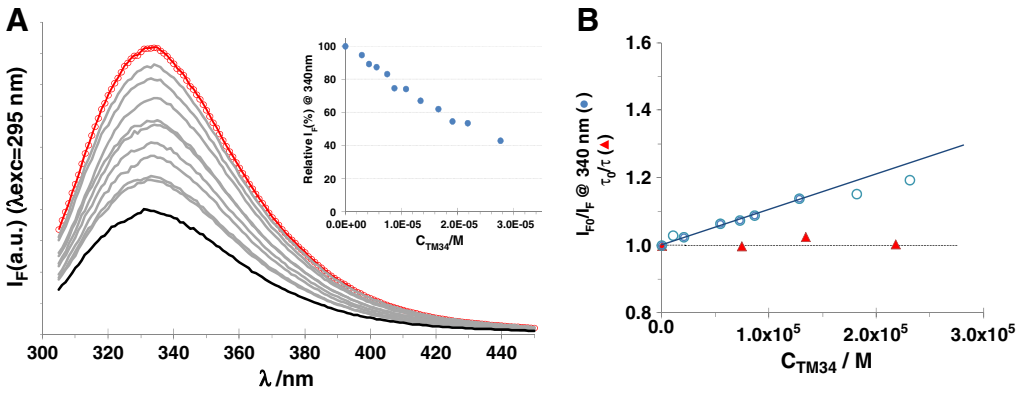

Fig. 4. Effect of TM34 in HSA fluorescence emission. A. Emission spectra ($\lambda_{exc}=295$ nm) of HSA in the absence (red open circles) and in the presence (line) of increasing concentrations of Ru-complex in 2% DMSO/10 mM Hepes pH 7.4/0.15 M NaCl ($C_{HSA}=1.2$ μM, $C_{TM34}=0$–27.6 μM, samples prepared individually and incubated for 3 h at 37 °C). *Inset*: change (%) in the emission intensity at $\lambda_{em}=340$ nm — data not corrected for inner filter effects. B. Stern–Volmer plots obtained at 340 nm for this system: I_{F0}/I_F for IFE corrected data (open circle), and $\bar{\tau}_0/\bar{\tau}$ (red closed triangles). Fluorescence measurements carried out after a 24 h incubation period (data not shown) yielded the same results as after a 3 h contact time. The Stern–Volmer linear fit for IFE corrected data (C_{TM34} in M) obeys ($R^2=0.9941$) $I_{F0}/I_F=(1.001\pm0.003)+(10.5\pm0.4)\times10^3\,C_{TM34}$.

a mechanism of static quenching. In other words, the fluorescence intensity of the solution decreases upon addition of a metal complex, but the fluorescence decay after pulse excitation is unaffected [71]. This is consistent with the formation of a non-fluorescent 1:1 adduct [71], according to the equilibrium

$$HSA+(TM34)\rightleftarrows\{(HSA)-(TM34)\}$$

with a binding constant K_B. In this case, Eq. (4) describes the variation of I_{F0}/I_F with C_{TM34},

$$\frac{I_{F0}}{I_F}=1+K_B[\text{complex}] \tag{4}$$

and the slope of the linear fit in the Stern–Volmer plot above can be interpreted as K_B (see Table 3) thus rendering $K_B=(10.5\pm0.4)\times10^3\,M^{-1}$, or $\log K_B=(4.02\pm0.02)$ and $K_D=95$ μM (K_D is the dissociation constant for the {(HSA)–(TM34)}adduct, or $1/K_B$).

The conditional binding constant of TM34 to HSA was also calculated by the computer program PSEQUAD [51] using the whole emission wavelength range (306–450 nm) – see Table 3 – and the calculated conditional binding constant is in good agreement with the result of the Stern–Volmer plot analysis.

Considering that the incubation time in ultrafiltration measurements (up to 40 min) was considerably lower than the contact time in fluorescence assays (3 h), data indicates that the complex TM34 is quickly picked up by the protein, and equilibrium conditions are attained quite fast. In addition, the very small changes detected in the UV–vis electronic spectrum of TM34 in the presence of the protein support the fact that the complex binds as the parent complex as a whole, with no loss of its co-ligands.

In conclusion, fluorescence data for TM34 indicates the formation of a ground-state non-fluorescent 1:1 {(Ru-complex)–protein} adduct, which is confirmed by the measurement of fluorescence lifetimes, and the stability constant calculated by fluorimetry confirms the value obtained by ultrafiltration–UV–vis.

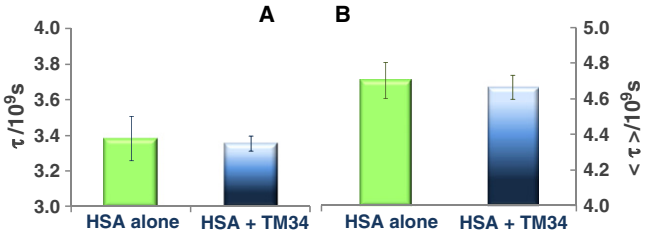

Fig. 5. Effect of TM34 in HSA fluorescence lifetime: A. Amplitude-weighted mean fluorescence lifetime ($\bar{\tau}_0$) in the absence and in the presence of the complex; B. mean fluorescence lifetime (<τ>) in the absence and in the presence of TM34 in 2% DMSO/10 mM Hepes pH 7.4/0.15 M NaCl. There are no significant differences in the fluorescence lifetime of the protein measured in the absence and presence of TM34 (averaged values of 3 independent samples).

3.5. Effect of HSA on cytotoxic activity of TM34

Serum proteins play a crucial role in the transport and delivery and are frequently involved in the mechanism of action of antitumoral metallodrugs [72,73]. Considering that a vast majority of therapeutical metal-containing compounds are administered intravenously, interactions with blood carrier proteins such as HSA can determine the overall drug biodistribution and affect the drug biological activity and toxicity. This crucial aspect, that has been frequently overlooked in the literature when screening the activity of prospective metallodrugs, is now being given due relevance in some recent reports [40,72,74]. In this context, experiments to evaluate if the binding of TM34 to HSA could influence the cytotoxic activity of the metal complex in the A2780 cell line, in comparison to the compound alone, were carried out. Data are shown in Fig. 6.

Several controls were used in these assays, namely cells with no treatment (negative control, identified as control in Fig. 6), cells treated with HSA alone (with 1, 5 and 10 μM (Fig. 6.A1/B) or with 5, 25 and 50 μM (Fig. 6.A2) protein concentration) and cells treated with TM34 in the absence of HSA (positive controls, TM34-1 μM and -5 μM in Fig. 6.A1 and A2, respectively).

Cell viability increases *ca.* 15% in the presence of HSA in the case of the A2780 cell line, while A2780cisR cell viability is less sensitive to the presence of the protein (Fig. 6.B). Pre-incubation with HSA did not influence significantly the effect of TM34 on the viability of both A2780 and A2780cisR cells, indicating that the activity of the complex remains relatively unaffected when bound to HSA. As such, TM34 can be transported in the blood stream by HSA and be delivered to target tissues while retaining its activity. Furthermore, given the fact that albumin accumulates in tumor tissues as a consequence of the EPR effect, this feature could provide a route for enhanced selectivity due to passive targeting by HSA.

4. Conclusions

The organometallic complex TM34, $[Ru^{II}Cp(bipy)(PPh_3)_2][CF_3SO_3]$, is a very promising large spectrum antitumor agent [75]. In addition

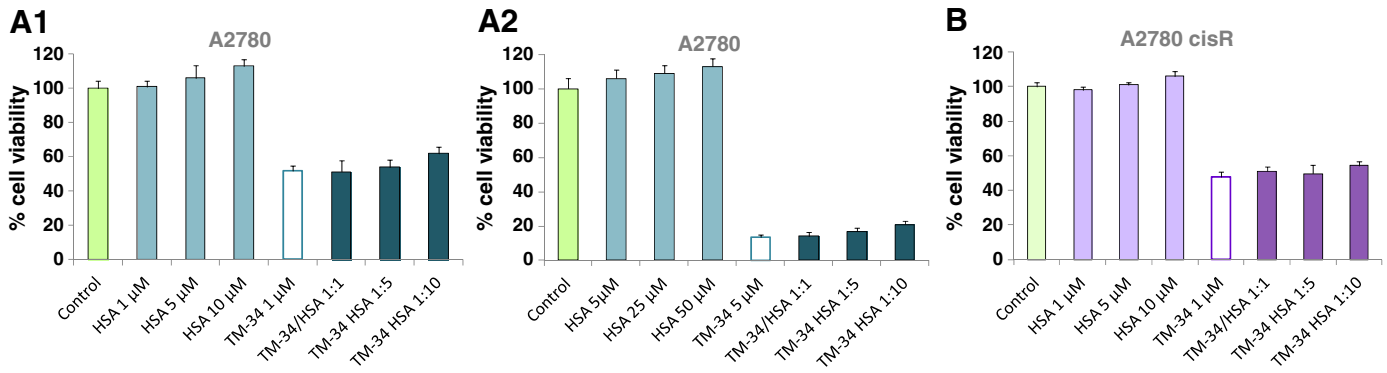

Fig. 6. Effect of HSA on the cytotoxicity of TM34 on A2780 (A) and A2780cisR cells (B) after a 24 h challenge. A2780 cells were treated with TM34 at 1 μM (A1 and B) and 5 μM (A2) pre-incubated with HSA at 1:1, 1:5 and 1:10 complex-to-protein molar ratios. Data shown are the mean values (±SD) of two independent experiments, each performed with at least six replicates. *Control* indicates cells with no treatment (negative control), HSA-5, -25 and -50 μM indicate cells treated with HSA alone in the concentrations indicated, TM34-1 μM and -5 μM are positive controls (cell treated with the complex in the absence of albumin).

to its activity against leukemia previously reported [28], it is also very active against a panel of cell lines representative of different tumor conditions, such as ovarian adenocarcinoma (CisPt sensitive and resistant), hormone dependent breast adenocarcinoma (ERα+) and prostate cancer. TM34 was found to be ~15 times more active against A2780 than the metallodrug in clinical use cisplatin. It is particularly active for cisplatin resistant cell lines, ~200-folds more cytotoxic against A2780cisR while also being 100-folds more active in the case of the more resistant MCF7 and PC3 cell lines. Moreover, its activity (measured as the IC_{50} value) towards the non-tumorigenic V79 cell line was 7-to-60-times lower (for PC3 and A2780cisR, respectively), which might suggest some intrinsic selectivity of TM34 to cancer cells.

Concerning its mode of action, TM34 is a strong PARP-1 inhibitor, its effect being comparable to that of some gold complexes [39]. The IC_{50} value surpasses that of the reference inhibitor, as well as the values reported for CisPt and the anti-metastatic Ru-complexes NAMI-A and RAPTA-T. To the best of our knowledge TM34 is the strongest PARP-1 inhibitor Ru-containing agent reported.

Distribution and delivery through the blood plasma should be possible since TM34 binds to human serum albumin forming a 1:1 adduct. The stability binding constant calculated for this {HSA–TM34} adduct (by ultrafiltration–UV–vis and by fluorescence data) was log $K_B' = 4$, which is similar to the constant found for KP1019 [40], and indicates that the complex can be transported in the blood stream by HSA.

The presence of albumin did not affect significantly the activity of TM34 against ovarian adenocarcinoma cells (either CisPt sensitive or resistant), indicating that the interaction with HSA does not deactivate the complex. This binding might provide a path to enhance the selectivity of TM34 by passive targeting to tumor tissues through HSA binding.

Abbreviations

bipy	2,2′-bipyridine
CisPt	cisplatin
Cp	η^5-cyclopentadienyl
Hepes	4-(2-hydroxyethyl)-1-piperazineethanesulfonic acid
IFE	inner filter effect
Im	imidazole
Ind	indazole
KP1019	indazolium bisindazoletetrachlororuthenate, [HInd][*trans*-$Ru^{III}Cl_4(Ind)_2$]
LMM	low molecular fraction (separated by ultrafiltration)
NAMI-A	[HIm][*trans*-$Ru^{III}Cl_4$(DMSO)Im]
PARP-1	poly(ADP-ribose) polymerase 1
PPh_3	triphenylphosphane
PTA	1,3,5-triaza-7-phosphaadamantane
RAPTA-T	[$Ru^{II}Cl_2(\eta^6$-toluene)(PTA)]
TM34	η^5-cyclopentadienyl(2,2′-bipyridyl)(triphenylphosphane) Ruthenium(II) triflate

Acknowledgments

This work was financed by Portuguese national funds through FCT, the Portuguese Foundation for Science and Technology within the scope of projects PTDC/QUI-QUI/101187/2008, FCT/DREBM 00521, PEst-OE/QUI/UI0100/2011, PEst-OE/QUI/UI0612/2011, PEst-OE/QUI/UI 536/2011, *Ciência2007* and *Ciência2008* Initiatives, grant SFRH/BD/45871/2008, and from the Hungarian–Portuguese Intergovernmental S&T Cooperation Programme (Proc.4.1.1 Hungria; OMFB-00494/2008; PT-19/07). T. Jakusch and É. A. Enyedy gratefully acknowledge the financial support of J. Bolyai Research Fellowship. A. I. Tomaz is thankful to Prof. S. B. Costa and Dr. S. Andrade (CQE-IST-UTL) for the free access to a spectrofluorometer to record part of the fluorescence data.

Appendix A. Supplementary data

Supplementary data to this article can be found online at http://dx.doi.org/10.1016/j.jinorgbio.2012.06.016.

References

[1] The World Health Organization website, http://www.who.int/mediacentre/factsheets/fs297/en/index.htmlaccessed on March, 15 2012.
[2] SEER Cancer Statistics, U.S. National Cancer Institute website, http://seer.cancer.gov/statfacts/html/all.htmlaccessed on March, 15 2012.
[3] B. Rosenberg, L. Vancamp, T. Krigas, Nature 205 (1965) 698–699.
[4] M. Galanski, V.B. Arion, M.A. Jakupec, B.K. Keppler, Curr, Pharm. Design 9 (2003) 2078–2089.
[5] L. Kelland, Nature Cancer Rev. 7 (2007) 573–584.
[6] W.H. Ang, P.J. Dyson, Eur. J. Inorg. Chem 20 (2006) 4003–4018.
[7] A. Levina, A. Mitra, P.A. Lay, Metallomics 1 (2009) 458–470.
[8] P.C.A. Bruijnincx, P.J. Sadler, Curr. Opin. Chem. Biol. 12 (2008) 197–206.
[9] G. Süss-Fink, Dalton Trans. 39 (2010) 1673–1688.
[10] E.S. Antonarakis, A. Emadi, Cancer Chemother. Pharmacol. 66 (2010) 1–9.
[11] A. Bergamo, C. Gaiddon, J.H.M. Schellens, J.H. Beijnen, G. Sava, J. Inorg. Biochem. 106 (2012) 90–99.
[12] C.G. Hartinger, M.A. Jakupec, S. Zorbas-Seifrieda, M. Groessl, A. Egger, W. Berger, H. Zorbas, P.J. Dyson, B.K. Keppler, Chem. Biodivers. 5 (2008) 2140–2155.
[13] E. Alessio, G. Mestroni, A. Bergamo, G. Sava, Curr. Topics Med. Chem. 4 (2004) 1525–1535.
[14] Y.K. Yan, M. Melchart, A. Habtemariam, P.J. Sadler, Chem. Commun. (2005) 4764–4776.
[15] C. Scolaro, A. Bergamo, L. Brescacin, R. Delfino, M. Cocchietto, G. Laurenczy, T.J. Geldbach, G. Sava, P.J. Dyson, J. Med. Chem. 48 (2005) 4161–4171.
[16] G. Gasser, I. Ott, N. Metzler-Nolte, J. Med. Chem. 54 (2011) 3, http://dx.doi.org/10.1021/jm100020w.
[17] P.C.A. Bruijnincx, P.J. Sadler, In: in: R. van Eldik, C.D. Hubbard (Eds.), Advances in Inorganic Chemistry, 61, Academic Press, London, 2009, pp. 1–62.

[18] P.J. Dyson, Nature 458 (2009) 389.
[19] M. Gras, B. Therrien, G. Süss-Fink, O. Zava, P.J. Dyson, Dalton Trans. 39 (2010) 10305–10313.
[20] R. Anand, J. Maksimoska, N. Pagano, E.Y. Wong, P.A. Gimotty, S.L. Diamond, E. Meggers, R. Marmorstein, J. Med. Chem. 52 (2009) 1602–1611.
[21] E. Meggers, G.E. Atilla-Gokcumen, K. Gründler, C. Frias, A. Prokop, Dalton Trans. (2009) 10882–10888.
[22] P. Xie, D.S. Williams, G.E. Atilla-Gokcumen, L. Milk, M. Xiao, K.S.M. Smalley, M. Herlyn, E. Meggers, R. Marmorstein, Chem. Biol. 3 (2008) 305–316.
[23] D.N. Akbayeva, L. Gonsalvi, W. Oberhauser, M. Peruzzini, F. Vizza, P. Brüggeller, A. Romerosa, G. Sava, A. Bergamo, Chem. Commun. (2003) 264–265.
[24] B.T. Loughrey, P.C. Healy, P.G. Parsons, M.L. Williams, Inorg. Chem. 47 (2008) 8589–8591.
[25] M.H. Garcia, A. Valente, P. Florindo, T.S. Morais, M.F.M. Piedade, M.T. Duarte, V. Moreno, F.X. Avilés, J. Loreno, Inorg. Chimica Acta 363 (2010) 3765–3775.
[26] M.H. Garcia, T.S. Morais, P. Florindo, M.F.M. Piedade, V. Moreno, C. Ciudad, V. Noe, J. Inorg. Biochem. 103 (2009) 354–361.
[27] V. Moreno, J. Lorenzo, F.X. Aviles, M.H. Garcia, J.P. Ribeiro, T.S. Morais, P. Florindo, M.P. Robalo, Bioinorg. Chem. Appl. (2010) 1–11, http://dx.doi.org/10.1155/2010/936834 (Article ID 936834).
[28] V. Moreno, M. Font-Bardia, T. Calvet, J. Lorenzo, F.X. Avilés, M.H. Garcia, T.S. Morais, A. Valente, M.P. Robalo, J. Inorg. Biochem. 105 (2011) 241–249.
[29] X. Riera, V. Moreno, C.J. Ciudad, V. Noe, M. Font-Bardía, X. Solans, Bioinorg. Chem. Appl. (2007) 1–15, http://dx.doi.org/10.1155/2007/98732.
[30] A. Casini, C. Gabbiani, F. Sorrentino, M.P. Rigobello, A. Bindoli, T.J. Geldbach, A. Marrone, N. Re, C.G. Hartinger, P.J. Dyson, L. Messori, J. Med. Chem. 51 (2008) 6773–6781.
[31] A. Bergamo, G. Sava, Dalton Trans. (2007) 1267–1272.
[32] A. Bindoli, M.P. Rigobello, G. Scutari, C. Gabbiani, A. Casini, L. Messori, Coord. Chem. Rev. 253 (2009) 1692–1707.
[33] V. Milacic, D. Fregona, Q.P. Dou, Histol. Histopathol. 23 (2008) 101–108.
[34] C.J. Lord, A. Ashworth, Curr. Opin. Pharmacol. 8 (2008) 363–369.
[35] S.J. Miknyoczki, S. Jones-Bolin, S. Pritchard, K. Hunter, H. Zhao, W.H. Wan, M. Ator, R. Bihovsky, R. Hudkins, S. Chatterjee, A. Klein-Szanto, C. Dionne, B. Ruggeri, Mol. Cancer Ther. 2 (2003) 371–382.
[36] S. Rottenberg, J.E. Jaspers, A. Kersbergen, E. van der Burg, A.O.H. Nygren, S.A.L. Zander, P.W.B. Derksen, M. de Bruin, J. Zevenhoven, A. Lau, R. Boulter, A. Cranston, M.J. O'Connor, N.M.B. Martin, P. Borst, J. Jonkers, P. Natl. Acad. Sci. USA 105 (2008) 17079–17084.
[37] B. Evers, R. Drost, E. Schut, M. de Bruin, E. van der Burg, P.W.B. Derksen, H. Holstege, X.L. Liu, E. van Drunen, H.B. Beverloo, G.C.M. Smith, N.M.B. Martin, A. Lau, M.J. O'Connor, J. Jonkers, Clin. Cancer Res. 14 (2008) 3916–3925.
[38] C.K. Donawho, Y. Luo, Y.P. Luo, T.D. Penning, J.L. Bauch, J.J. Bouska, V.D. Bontcheva-Diaz, B.F. Cox, T.L. DeWeese, L.E. Dillehay, D.C. Ferguson, N.S. Ghoreishi-Haack, D.R. Grimm, R. Guan, E.K. Han, R.R. Holley-Shanks, B. Hristov, K.B. Idler, K. Jarvis, E.F. Johnson, L.R. Kleinberg, V. Klinghofer, L.M. Lasko, X.S. Liu, K.C. Marsh, T.P. McGonigal, J.A. Meulbroek, A.M. Olson, J.P. Palma, L.E. Rodriguez, Y. Shi, J.A. Stavropoulos, A.C. Tsurutani, G.D. Zhu, S.H. Rosenberg, V.L. Giranda, D.J. Frost, Clin. Cancer Res. 13 (2007) 2728–2737.
[39] F. Mendes, M. Groessl, A.A. Nazarov, Y.O. Tsybin, G. Sava, I. Santos, P.J. Dyson, A. Casini, J. Med. Chem. 54 (2011) 2196–2206.
[40] J.C. Pessoa, I. Tomaz, Curr. Med. Chem. 17 (2010) 3701–3738.
[41] M. Fasano, S. Curry, E. Terreno, M. Galliano, G. Fanali, P. Narciso, S. Notari, P. Ascenzi, IUBMB Life 57 (2005) 787–796.
[42] The U.S. Food and Drug Administration website, http://www.fda.gov/OHRMS/DOCKETS/98fr/00n-1269-nfr0001-03.pdfretrieved on March, 15 2012.
[43] F. Kratz, J. Control. Release 132 (2008) 171–183.
[44] H. Maeda, Bioconjugate Chem. 21 (2010) 797–802.
[45] A. Sanz-Medel, T. Jakusch, D. Hollender, E.A. Enyedy, C.S. Gonzalez, M. Montes-Bayon, J.C. Pessoa, I. Tomaz, T. Kiss, Dalton Trans. (2009) 2428–2437.
[46] K. Hirayama, S. Akashi, M. Furuya, K. Fukuhara, Biochem. BiophRes. Co 173 (1990) 639–646.
[47] L. Vellenga, T. Wensing, H.J.A. Egberts, J.E. Vandijk, J.M.V.M. Mouwen, H.J. Breukink, Vet. Res. Commun. 13 (1989) 467–474.
[48] B. Yuan, K. Murayama, H. Yan, Appl. Spectrosc. 61 (2007) 921–927.
[49] A. Coutinho, M. Prieto, J. Chem. Ed. (1993) 425–428.
[50] Bernard Valeur, In: Molecular Fluorescence: Principles and Applications, Wiley-VCH Verlag GmbH, 2001, pp. 159–165, Chap. 6.
[51] L. Zekany, I. Nagypal, In: in: D. Leggett (Ed.), Computational Methods for the Determination of Stability Constants, Plenum Press, York, 1985, pp. 291–353.
[52] É.A. Enyedy, E. Farkas, O. Dömötör, M.A. Santos, J. Inorg. Biochem. 105 (2011) 444–453.
[53] T. Mosmann, J. Immun. Meth. 65 (1983) 55–63.
[54] S. Gama, F. Mendes, F. Marques, I.C. Santos, M.F. Carvalho, I. Correia, J.C. Pessoa, I. Santos, A. Paulo, J. Inorg. Biochem. 105 (2011) 637–644.
[55] A. Bergamo, A. Masi, A.F.A. Peacock, A. Habtemariam, P.J. Sadler, G. Sava, J. Inorg. Biochem. 104 (2010) 79–86.
[56] V. Schreiber, F. Dantzer, J.C. Ame, G. de Murcia, Nat. Rev. Mol. Cell Bio. 7 (2006) 517–528.
[57] T. Helleday, E. Petermann, C. Lundin, B. Hodgson, R.A. Sharma, Nat. Rev. Cancer 8 (2008) 193–204.
[58] M.Y. Kim, T. Zhang, W.L. Kraus, Gene Dev. 19 (2005) 1951–1967.
[59] S. Homburg, L. Visochek, N. Moran, F. Dantzer, E. Priel, E. Asculai, D. Schwartz, V. Rotter, N. Dekel, M. Cohen-Armon, J. Cell Biol. 150 (2000) 293–307.
[60] Z. Herceg, Z.Q. Wang, Mutat. Res.-Fund. Mol. M. 477 (2001) 97–110.
[61] R.K. Amaravadi, C.B. Thompson, Clin. Cancer Res. 12 (2007) 7271–7279.
[62] M. Serratrice, F. Edafe, F. Mendes, R. Scopelliti, S.M. Zakeeruddin, M. Grätzel, I. Santos, M.A. Cinellu, A. Casini, Dalton Trans. 41 (2012) 3287–3293.
[63] A. Mangerich, A. Bürkle, Int. J. Cancer 128 (2011) 251–265.
[64] N.J. Curtin, Expert Rev. Mol. Med. 7 (2005) 1–20.
[65] Joseph R. Lakowicz, In: Principles of Fluorescence Spectroscopy, 3rd ed., Springer, New York, 2006, pp. 530–573, Chap.16.
[66] G. Sudlow, D.J. Birkett, D.N. Wade, Mol. Phamacol. 11 (1975) 824.
[67] G. Sudlow, D.J. Birkett, D.N. Wade, Mol. Phamacol. 12 (1976) 1052.
[68] W. Bal, J. Christodoulou, P.J. Sadler, A. Tucker, J. Inorg. Biochem. 70 (1998) 33–39.
[69] Joseph R. Lakowicz, In: Principles of Fluorescence Spectroscopy, 3rd ed., Springer, New York, 2006, pp. 63–94, Chap. 3.
[70] Joseph R. Lakowicz, In: Principles of Fluorescence Spectroscopy, 3rd ed., Springer, New York, 2006, pp. 278–327, Chap. 8.
[71] Bernard Valeur, In: Molecular Fluorescence: Principles and Applications, Wiley-VCH Verlag GmbH, 2001, pp. 72–90, Chap. 4.
[72] A.R. Timerbaev, C.G. Hartinger, S.S. Aleksenko, B.K. Keppler, Chem. Rev. 106 (2006) 2224–2248.
[73] I. Kostova, Curr. Med. Chem. 13 (2006) 1085–1107.
[74] E.A. Enyedy, L. Horváth, A. Hetényi, T. Tuccinardi, C.G. Hartinger, B.K. Keppler, T. Kiss, Bioorg. Med. Chem. 19 (2011) 4202–4210.
[75] M.H. Garcia, T.S. Morais, A.I. Tomaz, F. Marques, F. Mendes, Patent application PT105890.